Magnetophoresis of Nanoparticles

JitKang Lim,*,†,∥ Caitlin Lanni,‡ Eric R. Evarts,‡ Frederick Lanni,§ Robert D. Tilton,†,⊥ and Sara A. Majetich*,‡

†Department of Chemical Engineering, ‡Physics, §Biological Sciences, ⊥Biomedical Engineering, Carnegie Mellon University, Pittsburgh, Pennsylvania 15213, United States, and ∥School of Chemical Engineering, Universiti Sains Malaysia, 14300 Seberang Prai Selatan, Penang, Malaysia

ARTICLE

ABSTRACT Iron oxide cores of 35 nm are coated with gold nanoparticles so that individual particle motion can be tracked in real time through the plasmonic response using dark field optical microscopy. Although Brownian and viscous drag forces are pronounced for nanoparticles, we show that magnetic manipulation is possible using large magnetic field gradients. The trajectories are analyzed to separate contributions from the different types of forces. With field gradients up to 3000 T/m, forces as small as 1.5 fN are detected.

KEYWORDS: magnetophoresis · magnetic nanoparticles · motion control · surface plasmon resonance · Brownian motion.

Real-time manipulation of nanoscale objects without direct contact poses many challenges. The trajectories of larger particles may be controlled by fluid flow or by electric or magnetic fields. With nanoparticles there are large viscous drag and Brownian forces that impede fluid flow, and the electrical or magnetic forces are much weaker. Motion can be controlled to some extent by chemical binding affinity, but this tends to be irreversible, and it relies on diffusion rather than deterministic motion. Understanding the requirements for remote manipulation of nanoparticles is of particular interest both for cell biology, where the particle could be moved within a living cell, and for microfluidics, where the use of nanoparticles instead of micrometer-scale beads could lead to greater dynamic range in the detection sensitivity.

There are several options for controlling the motion of nanoparticles. Chemical affinity works to some extent, but the binding events tend to be irreversible. Optical tweezers can grasp and release particles as small as a few nanometers, while the motion is tracked by either the surface plasmon resonance (SPR) or fluorescence.[1−3] However, this technique has a limited manipulation area due to tight focusing requirements,[4] and it would be difficult to incorporate into a microfluidic system.[5] Magnetic micromanipulation of nanoscale objects offers an alternative, minimally invasive, and scalable approach. Magnetic tweezers have already been used with micrometer-sized magnetic beads to measure the elasticity of single DNA molecules,[6] the local viscoelasticity of the cytoplasm,[7] and the mechanical properties of chromatin in living cells,[8] and for ion channel activation.[9] In experiments where particles interact with living cells, there is a complex biochemical response in addition to the application of a magnetic force; smaller particles would be beneficial if they caused less of an unintentional response. There are two critical challenges in controlling the transport behavior of nanofeatures: (1) sufficient force to induce their movement and (2) a visualization scheme to track their motion. Here we address these issues and demonstrate the conditions for magnetically driven capture and release of magnetic-plasmonic nanoparticles while simultaneously monitoring the individual particle trajectories using dark field optical microscopy.[10]

Controlled guidance is challenging because the magnetic, viscous drag, and random Brownian forces scale differently with the particle size.[11,12] The magnetic force is proportional to the volume of the magnetic core, $\sim D_{mag}^3$, while the viscous drag force scales with the hydrodynamic diameter, D_H, so it is harder to move smaller particles. In addition, small particles are more susceptible to Brownian motion.[10] Since the average size of a Brownian displacement is proportional to $D_H^{-1/2}$, small particles will have larger random steps during magnetophoresis, making them harder to track. The magnetic force is proportional to the gradient of the external magnetic field.[13] Thus, large field gradients must be employed, and larger particle sizes will always provide

*Address correspondence to chjitkangl@eng.usm.my, sm70@andrew.cmu.edu.

Received for review September 13, 2010 and accepted December 03, 2010.

Published online December 9, 2010. 10.1021/nn102383s

greater magnetic responsiveness than smaller versions of the same particle. Nevertheless, magnetic nanoparticles potentially hold great advantages over their micrometer sized counterparts, especially for measuring the physical and chemical properties of cellular components in the size range of a few to a few hundred nanometers. Only particles smaller than ~200 nm are drawn into cells by endocytosis without causing adverse effects.[14,15] Nanoparticles would require lower magnetophoretic forces,[16] and it is hypothesized that there would be fewer local obstructions to the particle motion as they move across the cytoplasmic network.[16]

Most previous magnetophoretic motion control studies on sub-100 nm particles focused on the collective magnetic manipulation of a swarm of nanoparticles.[17,18] However, the behavior of individual particles is important for many microscale studies, such as microfluidic sorting and investigation of processes within single cells. Here we explore real-time magnetophoretic motion control of single nanosized particles and develop a quantitative analysis scheme to distinguish the magnetic, drag, and thermal influences on their trajectories.

Quantitative biomechanics measurements require particles that are monodisperse in size and magnetization, so that they experience the same magnetophoretic force for a given high-field gradient. The nanoparticles should therefore be superparamagnetic in order to minimize aggregation due to magnetostatic interactions. For magnetite (Fe_3O_4) particles, the superparamagnetic size limit is ~35 nm in diameter,[19] and this sets the size limit on the magnetic nanoparticles employed in this study. Moreover, there must be a signal that allows individual nanoparticles to be tracked in real time, which can be achieved by either fluorescent or plasmonic labeling.

Methods for creating high magnetic field gradients could be adapted to microfluidic systems[20,21] appropriate for subcellular measurements, including lithographically fabricated micrometer-sized magnetic patterns, which are magnetized to manipulate micrometer-scale particles,[16,22] and arrays of current-carrying wires, which can control the position of swarms of magnetic nanoparticles.[17] The relatively small magnetic moment of the nanoparticles, which were typically 10−30 nm in size, has been the main limitation on F_{mag}.

There are well-established optical methods for tracking particle motion. While larger particles are followed individually with conventional bright field microscopy, nanoparticles must be tracked indirectly. The magnetic nanoparticle could be tagged with a fluorescent molecule or quantum dot[21,23] or with a gold or silver nanoparticle with a surface plasmon resonance in the visible region. Quantum dot-labeled 4 nm magnetite particles (σ_s ~3 emu/g) have been moved magnetically within living cells subjected to a small permanent magnet with a surface magnetic field of ~3000 G.[18] However, the magnetophoretic response was very slow, with speeds on the order of μm/hour, due not only to the relatively small magnetic field gradient of a permanent magnet but also to the significant effect of thermal displacement on small nanoparticles. Three-pole magnetic tweezers have been used to generate magnetic field gradients up to 8000 T/m, applying a magnetic force of 5 pN to move 350 nm iron oxide particles 3.5 μm in 1.5 s within a cell.[16]

Here we describe a single magnetic tip that can controllably collect and release magnetic-plasmonic particles with an iron oxide core 38 nm in diameter and a 67 nm thick polymer/Au nanoparticle plasmonic shell. Dark field optical microscopy is used to observe the plasmonic scattering of individual particles as they move within an aqueous dispersion under the combined influence of magnetic, viscous drag, and Brownian forces. The trajectories are analyzed quantitatively to differentiate the effects of these forces and to reveal the requirements for magnetic manipulation of nanoparticles within microfluidic devices or living cells. Moreover, since the magnitude of the forces acting on the nanoparticles is quite small, this technique also establishes a method for detecting tiny forces such as those that might occur during the binding events of molecular species attached to the nanoparticles. We describe the real-time imaging of magnetic nanoparticle capture and release using highly localized magnetic field gradients. Analysis of the magnetophoretic trajectories of individual particles provides a map of the local magnetophoretic force and associated field gradient. With this analysis technique, it is possible to detect magnetic forces as small as 1 fN.

RESULTS AND DISCUSSION

We prepared negatively charged magnetic-plasmonic nanoparticles with polymer-coated iron oxide cores and a shell of gold particles attached to the polymer, as summarized in Figure 1. (For synthetic details see the Methods section.) Figure 1a and b show TEM micrographs of the mainly magnetite iron oxide particle before and after the decoration with 1−3 nm gold clusters. Figure 1c shows a magnified view of a single gold-coated iron oxide core particle. The individual black dots in Figure 1c correspond to single gold clusters.[25] After the gold coating, the particle suspension has a surface plasmon resonance at 523 nm. (See Supporting Information for absorption spectra.) The diameter of the iron oxide core obtained from transmission electron microscopy (TEM) images, $D_{mag} = 37.6 \pm 3.8$ nm, compared well with a size of 10−15 nm for most monodisperse magnetic nanoparticles studied previously.[18,25] The specific saturation magnetization was 76.1 emu/g Fe_3O_4, slightly lower than that for bulk magnetite. (See Supporting Information for magnetometry data.) The large particle size employed here together with its high saturation magnetization, theoreti-

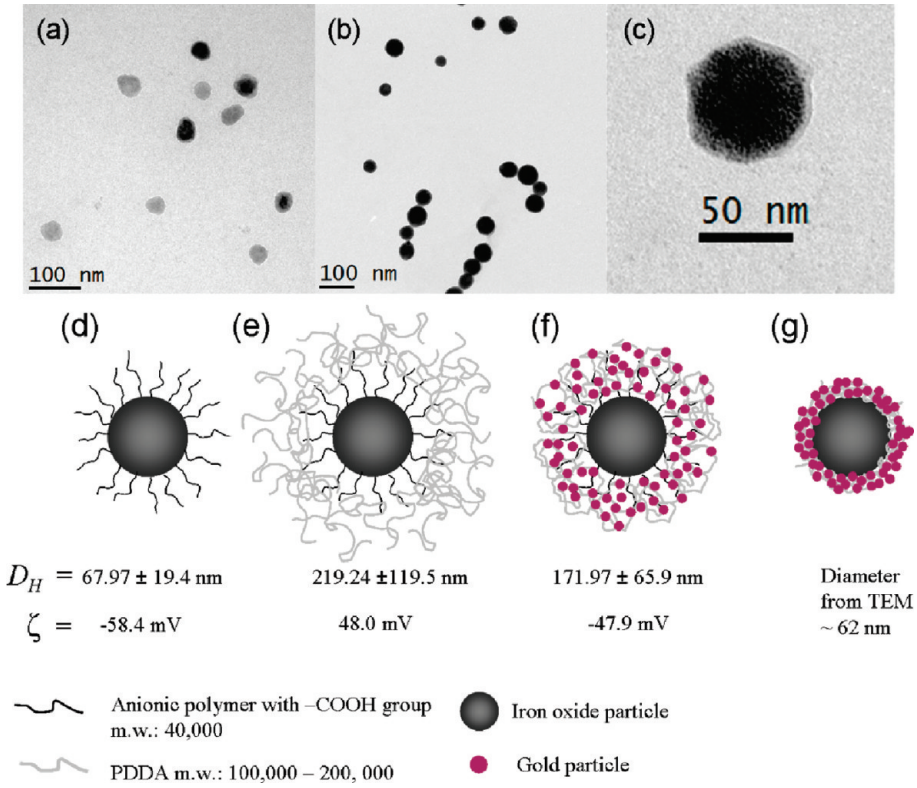

Figure 1. (a−c) Transmission electron micrographs of the magnetic plasmonic nanoparticles at different stages of the coating process. (a) polymer-coated ~35 nm iron oxide core nanoparticles, (b) nanoparticles after decoration with small gold particles, (c) magnified image of a single iron oxide core, gold shell particle. (d−f) Schematics of a particle in water, at different stages of the coating process, with corresponding experimental values of the average hydrodynamic diameter D_H and zeta potential ζ determined from dynamic light scattering. (d) An iron oxide particle, as received, (e) after coating with PDDA to reverse the surface charge and make the particle attractive to negatively charged gold seed clusters, (f) after decoration with gold, and (g) after drying so that the polymer collapses and the gold clusters are drawn close to the iron oxide core, as in the TEM images (b) and (c). The distributions of D_H for (d−f) can be found in the Supporting Information, Figure III.

cally, would lead to a larger magnetic force compared to that in previous studies,[18,25] since

$$\overrightarrow{F_{mag}} = (M_s V_{mag} \cdot \nabla)\vec{B} \quad (1)$$

where M_s is the saturation magnetization of particles at 396 emu/cm^3, V_{mag} is the particle volume at 2.79 × 10^{-23} m^3, and B is the magnetic induction. The particles are single magnetic domains and are therefore saturated in some direction. When in solution, they are free to rotate in order to align with their moments parallel to the applied field. Thermal fluctuations could lead to some temporary misalignment, and the equations quoted here are based on full alignment and are therefore upper bounds to the magnetic forces.

The hydrodynamic diameter D_H,which is the effective particle size that dictates the viscous drag and Brownian motion, was determined from dynamic light scattering (DLS). Figure 1d and e illustrate how D_H evolves as the core−shell structure is formed. Because the zeta potential of the initial particles is negative, they are coated with cationic poly(diallyldimethylammonium chloride) (PDDA) to promote the attachment of small negatively charged gold clusters. The hydrodynamic diameter after PDDA absorption (Figure 1e) is consistent with expectations for a single layer of adsorbed PDDA, which has a mean square radius of gyration of 32.8 to 47.2 nm for a molecular weight of 100 000−200 000.[26] D_H is reduced after gold decoration because the dense gold seeding causes the extended PDDA layer to partly collapse. When the particle dispersion is dried on a TEM grid for microscopy analysis (Figure 1f), the polymer shell collapses, and the observed size does not reflect the true D_H. For the particles used in the aqueous dispersion magnetophoresis experiments, D_H = 172 ± 66 nm.

The magnetic field gradient ∇B was generated using a triangular piece of a thin (5 μm) sheet of mu metal, a magnetically soft nickel iron alloy with a low coercivity, ~20 Oe,[27] and a saturation induction of 7.5 kG.[28] The sharp end of the tip was placed in an aqueous dispersion containing the nanoparticles and the blunt end in contact with the core of a solenoid. (See the Supporting Information for a detailed description of the magnetic tip apparatus.) When current passed through the solenoid coil, the mu metal tip was magnetized, and when the current was turned off, the tip rapidly demagnetized. (See the Supporting Information for details of the domain structure within the demagnetized tip.)

Dark field optical microscopy was used to image the surface plasmon resonance of individual particles

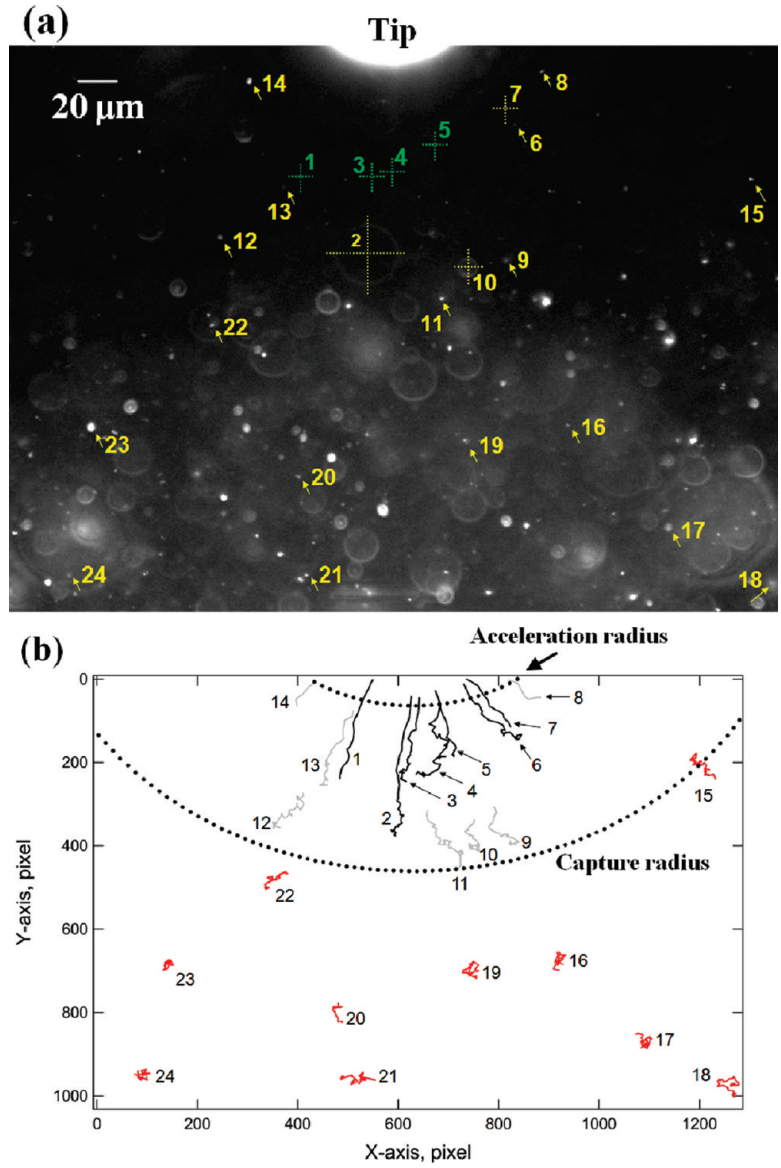

Figure 2. (a) Dark field optical micrograph showing the initial positions of multiple particles relative to the mu metal tip. (b) Trajectories of nanoparticles undergoing mainly diffusion (red), those undergoing magnetophoresis without acceleration (gray), and those showing some acceleration toward the magnetic field source (black).

as a function of time. Details of this technique have been described previously.[25] Figure 2a shows a dark field optical micrograph showing the initial positions of multiple particles, which appear as spots. The bright object at the top-center is the end of the mu metal tip. The trajectories of 24 individual particles were followed for a period of 25 s and analyzed to understand the magnetic, viscous drag, and random Brownian forces that affect their motion. Due to the fast depletion of nearby particles when the tip was magnetized, image analyses were performed on two dark field movies taken under the same conditions. The crosses in Figure 2a and numbers in green indicate the starting positions of particles from the second movie. Figure 2b shows a summary of the trajectories. For this combination of particle, field gradient, and observation time, there were two qualitatively different regimes. When the solenoid was energized, generating a large field gradient, nearby particles (#1−14) migrated toward the tip. Particles farther than 139 μm from the tip edge (#15−24) had no obvious net drift toward the tip.

These trajectory data were analyzed in order to differentiate the magnetophoretic and Brownian motion regimes. Random walk analysis was performed on the trajectories of particles 15−24, which were the least affected by the magnetic force.[25] The mean square displacement, $\langle x^2 \rangle$, for a known time step t was used to calculate the corresponding Brownian two-dimensional diffusion coefficient D:

$$\langle x^2 \rangle = 4Dt \qquad (2)$$

The average diffusion coefficient for the entire trajectory, D_{av}, was found from the results for all time steps in a trajectory, and the Stokes−Einstein equation was

used to determine the hydrodynamic diameter of the particle:

$$D_H = \frac{k_B T}{3\pi\eta D_{av}} \quad (3)$$

Here k_B is the Boltzmann constant, $T = 298$ K, and η is the viscosity of water, 0.00089 Pa · s. This analysis gave an average D_H of 163 nm, in good agreement with the average D_H of 172 nm found from DLS, which indicates that most of the spots correspond to single particles. (See the Supporting Information for complete size information.) In the diffusive regime, random Brownian forces act on particles, and their motion is impeded by viscous drag forces,

$$F_{drag} = 3\pi\eta D_H v \quad (4)$$

where v is the particle velocity. The standard deviation of the hydrodynamic radius (172 ± 66) is 38% of the average diameter, and this uncertainty will dominate the error in the.calculated F_{drag}. While F_{mag} is balanced by F_{drag}, with no particle acceleration, the average magnetophoretic velocity can be calculated by combining eqs 1 and 4:

$$v = (F_{mag}/3\pi\eta D_H) \quad (5)$$

Knowing the contributions from viscous drag and Brownian forces enables more quantitative analysis of magnetophoresis. Figure 3 shows typical trajectories of two particles within the capture radius, where there is magnetophoresis (particles 2 and 12), and one from outside it, which has mainly Brownian motion (particle 19). The velocity at each time step was decomposed into $v_{parallel}$, the velocity of the particle parallel to the magnetophoretic reference axis, and $v_{perpendicular}$, the velocity perpendicular to it. $v_{perpendicular}$ will be dominated by Brownian diffusion, while $v_{parallel}$ will have a combination of diffusion and magnetophoresis. We assumed that the absolute magnetophoretic displacement of the particle was along the field lines emanating from the surface of the tip. The optimum angle of this magnetophoretic pathway (the straight red line shown in Figure 3a and b) was determined by requiring that the sum of the $v_{perpendicular}$ was equal to zero. With respect to this optimized reference axis we calculated $v_{parallel}$ and $v_{perpendicular}$ for each time step using this algorithm. In Figure 3a and b, there is magnetophoresis, while in Figure 3c there is not. If the end of the tip acted as a point dipole, the particle trajectories would focus toward a single point. Instead, the reference axis results were consistent with field lines that emanated outward perpendicular to the surface of the tip. Because the field gradients are large near the corners of a ferromagnet, the upper edge corner of the wedge-shaped tip is likely to dominate the field gradient sensed by the nanoparticles.

The average viscous and Brownian forces are independent of position, while the magnetic force increases as the particles get closer to the tip, so particles will eventually start accelerating toward the tip. Particles such as particle 2 (Figure 4a) that get into this acceleration zone, here 15 μm from the tip surface, have increasing $v_{parallel}$ at each time step as they approach the tip. In contrast, particle 12 shows no evident magnetophoretic acceleration (Figure 4b). The capture and acceleration radius together give the spatial range of magnetophoretic control for a given time window. Particles 1−7 undergo acceleration at some point in their trajectories, while particles 8−14 do not. The average acceleration of particles 1−6 was ~10 μm/s^2, with 7 μm/s^2 for particle 7, and the average velocity before the acceleration for particles 1−7 ranged from 2 to 8 μm/s. In the terminal velocity region outside the acceleration zone, the average magnetic field gradient can be calculated. Here the drag force opposing the magnetic force is proportional to $v_{parallel}$, and $F_{drag} = F_{mag}$. The average terminal velocity for particles 8−13 varied from 0.9 to 7 μm/s, slightly lower than for particles 1−7, with the exception of particle 14, with a terminal velocity of 10 μm/s. Here the average magnetic field gradient ranged from 139 to 1533 T/m. Similar analysis can be used to estimate field gradients in the acceleration region, where $ma = F_{mag} - F_{drag}$. Here m is the mass of the particle and a is the acceleration found from the plot of $v_{parallel}$ versus time. The average magnetic field gradient in the acceleration region ranged from 1300 to 3000 T/m. A table with the results for all particles can be found in the Supporting Information. Within the "constant velocity" region, the nanoparticles experienced average magnetophoretic forces ranging from 1 to 20 fN, while F_{mag} was as high as 50 fN in the acceleration region. The ability to detect forces in this range could someday enable magnetic nanoparticles to probe protein-mediated DNA looping.[29]

Figure 4c shows how $v_{parallel}$ depends on the distance from the tip surface, for all particles tracked in a 50 time step (25 s) window. When the magnetic and drag forces are balanced, there is no acceleration. However, we observed rapid increases in $v_{parallel}$ as the particles approached the mu metal tip. Even at 160 μm away there is a net positive value of $v_{parallel}$. The results obviously depend on the duration of the observation, but they indicate that magnetophoresis exists even when short time trajectories appear to show Brownian diffusion. This is consistent with previous observations of slow magnetic capture of nanoparticles over macroscopic distances.[18,30] The new results show the threshold for increased velocity and acceleration, where real-time manipulation becomes feasible. $v_{parallel}$ begins to increase systematically at ~40 μm from the tip, and a more dramatic change is witnessed at or below 15 μm. Deterministic motion, where magnetophoresis domi-

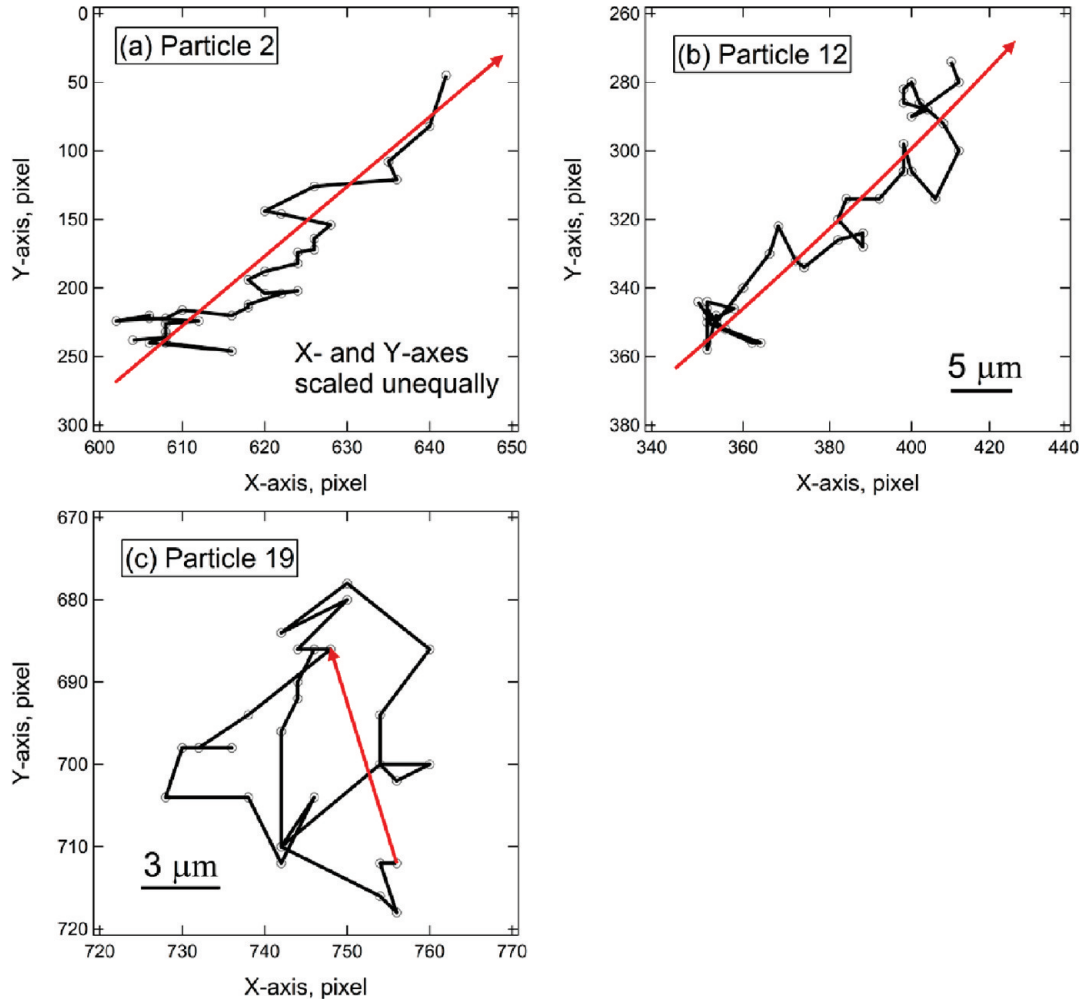

Figure 3. Individual trajectories of three particles. Note that the *x*- and *y*-axes are scaled unequally. The red arrows in (a) and (b) indicate the reference axes determined from analysis of the trajectories. Particle 2 (a) and particle 12 (b) show net magnetophoresis, while particle 19 (c) does not.

nates Brownian forces, requires field gradients greater than 1500 T/m.

To be useful in manipulation, magnetic tweezers must be able to both capture and release particles. After determining the criteria for magnetophoretic capture, we also examined the nanoparticle dynamics after they were released by switching off the solenoid. Since the particles are superparamagnetic and their thick polymer coating minimizes clustering, Brownian diffusion forces should dominate if the magnetic forces are diminishingly small. Figure 5 shows a series of dark field optical micrographs of the particles after release from the side of the mu metal tip over a period of 12 s. The side rather than the end of the mu metal tip was used because it provides improved statistics for the number of released particles and simplifies the diffusion calculation, making it one-dimensional in the distance from the tip edge. As shown in Figure 5, at 0 s, the particles are not distributed uniformly over the tip edge. This becomes more obvious after the solenoid current was turned off and the particles retreat from the mu-metal surface. Domain walls perpendicular to the side of the tip are most likely responsible for the variations in particle density. Magnetic force microscopy (see Supporting Information) of the mu metal tip in its demagnetized state shows multiple domains, with a characteristic size on the order of 0.5−1 μm. Because domain walls can be moved by a magnetic field,[31] particles could be selectively transported along a magnetic element by the force due to a moving domain wall, perhaps within a microfluidic device.[32,33] The MFM results showing stripe domains (see Supporting Information) and the observation that particles are not migrating toward the tip after the field is removed support our assertion that it is demagnetized. We anticipate that particles would migrate to the domain walls in the demagnetized tip, but we did not observe this for our combination of particle and tip materials.

The experimental particle flux data were compared with predictions for diffusion. According to Fick's law, the concentration of particles c will depend on the distance x from the tip surface and the time t after diffusion begins. Because DLS shows a distribution of hydrodynamic diameters, $D_{H,i}$, each with a size-dependent

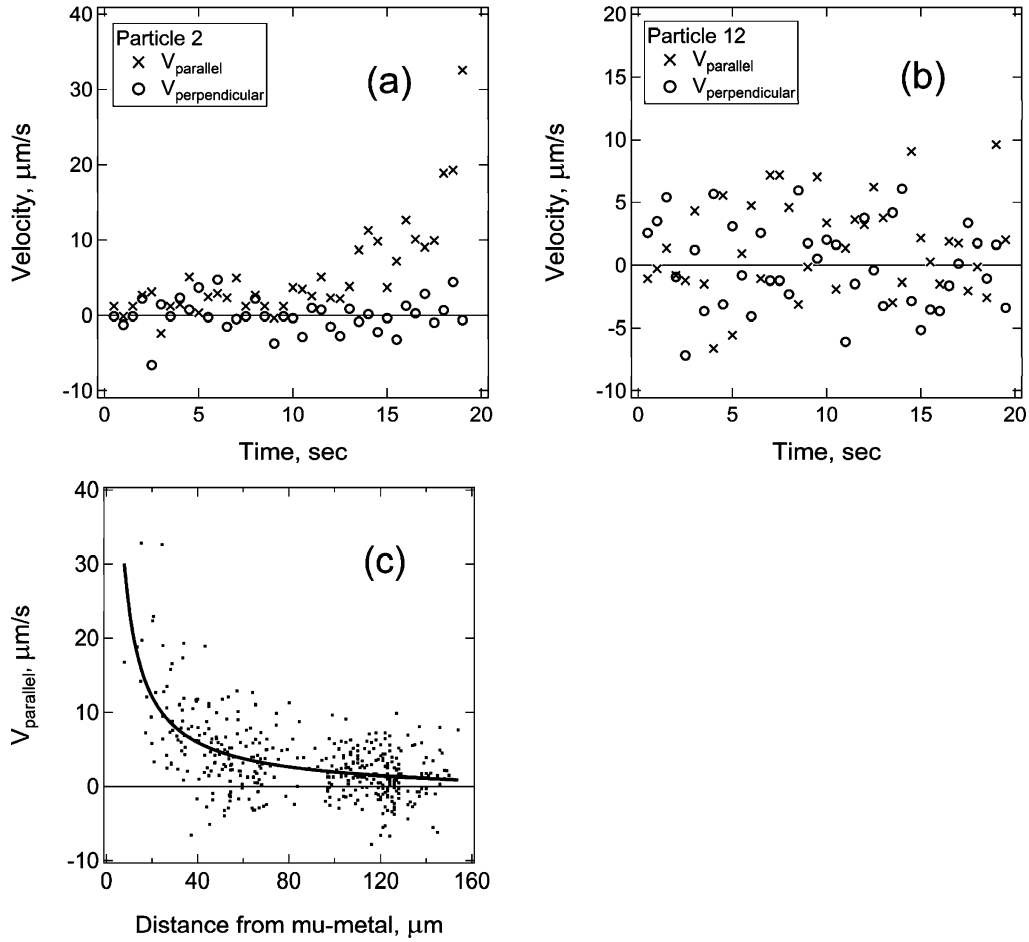

Figure 4. Decomposed parallel and perpendicular velocities for (a) particle 2 and (b) particle 12 with respect to the reference axis. After ~10 s, $v_{parallel}$ for particle 2 rises steadily, indicating acceleration. The average $v_{parallel}$ for particle 2 before noticeable acceleration is 3.6 μm/s, whereas for particle 12 it is 1.5 μm/s. (c) Scatter plot of all $v_{parallel}$ for particles 1−14, with a solid line to guide the eye. Notice that even at very low separation distance, <40 μm, $v_{parallel}$ can still be negative, indicating the strong influence of thermal randomization energy.

diffusion coefficient D_i, we assume a set of independent diffusion equations,

$$\frac{\partial c_i}{\partial t} = D_i \frac{\partial^2 c_i}{\partial x^2} \tag{6}$$

one for each particle size *i*. (Refer to the Supporting Information for the DLS size distribution.) Equation 6 is subjected to the boundary conditions that

$$\text{at } t = 0 \text{ and } x = 0,\ c_{0,i} \sim f_i\left(\frac{I_0}{(D_{H,i})^6}\right) \tag{7a}$$

$$\text{at } t = 0 \text{ and } x = \infty,\ c_{\infty,i} \sim f_i\left(\frac{I}{(D_{H,i})^6}\right) \tag{7b}$$

$$\text{and at } t = 0 \text{ and } x > 0, c_i = 0 \tag{7c}$$

Here I_0 and I are the average intensities obtained from the dark field micrograph at the mu metal edge and far away from it, respectively. f_i is the relative percentage of particles with hydrodynamic diameter $D_{H,i}$. In both DLS and dark field optical microscopy, the detected signal is due to particle scattering and is therefore proportional to D_H^6. Assuming the concentration of the particles is directly proportional to its intensity ($c_i = \alpha I_i$) and the proportionality constant α cancels after substituting into eq 6, the calculated results are in the units of intensity over D_H^6. For these particles where the gold is attached at the outermost surface, the plasmonic shell diameter is equal to the hydrodynamic diameter. The particle intensity concentration was obtained by normalizing the measured intensity to account for this size dependence. The total intensity was estimated using

$$I_{total}(r, t) = \sum_{i=1}^{n} D_{H,i}{}^6 I_i(x, t) \tag{8}$$

with no fitting parameters. Figure 6 compares the calculated intensity obtained from image analysis of the dark field optical micrographs shown in Figure 5, using ImageJ freeware.[34] At 12 s, the calculated result varies slightly from the data (see Supporting Information for details). Since the particles were initially highly concentrated, the independent diffusion assumption may not be completely accurate. Moreover, the average iron ox-

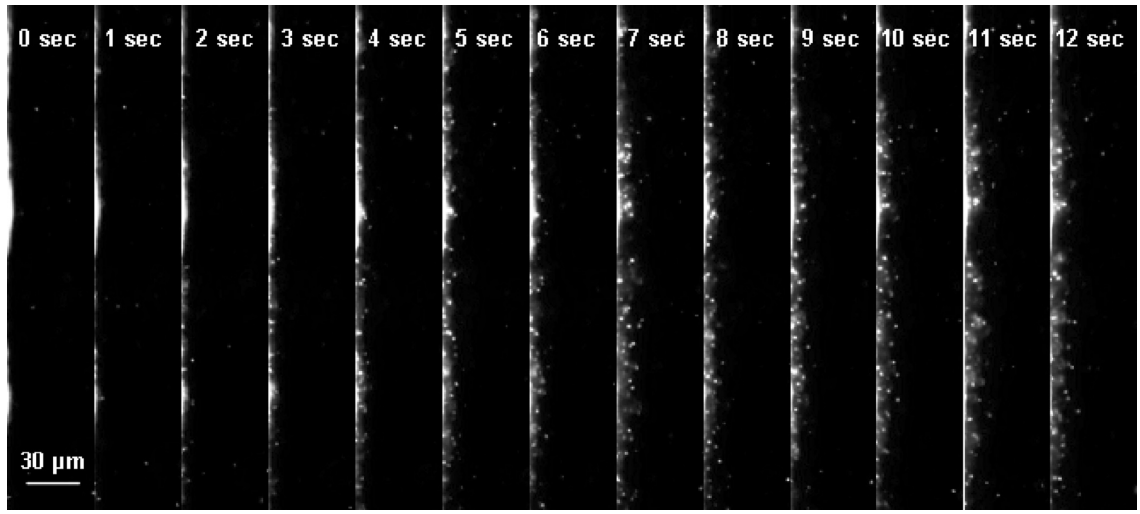

Figure 5. Particles released from the side of the mu metal tip after the solenoid current was switched off, as function of time. The mu metal is located on the left-hand side of each image.

ide core size of 37.6 ± 3.8 nm is very close to the ideal superparamagnetic limit of magnetite particles of 35 nm.[19] If some large particles are magnetically stable, the particles need not diffuse independently.

CONCLUSIONS

We have demonstrated the ability to magnetically capture and release individual nanoparticles with a 38 nm magnetic core in diameter and a 67 nm thick polymer/Au nanoparticle plasmonic shell. Highly localized large magnetic field gradients and the initial positions of the nanoparticles with respect to the magnetic source are crucial for real-time magnetic motion control. Analysis of the trajectories observed using dark field optical microscopy revealed a capture range; particles within this distance from the magnetized mu metal tip underwent noticeable magnetophoresis within 25 s. The magnetic field gradients within this region ranged from 100 to 1000 T/m and were sufficient for magnetophoresis to dominate Brownian motion. As the particles migrated closer to the magnetic field source, where the estimated field gradients were 1300−3000 T/m, the particles showed more deterministic trajectories. These results reveal how deterministic magnetic and viscous forces, combined with random Brownian forces, affect the trajectories of magnetic nanoparticles.

The quantitative analysis of the trajectories provides important feedback for the design of magnetic tweezers for manipulation of nanoparticles both in microfluidic systems and within living cells. Similar techniques could be used, but within a cell the local viscosity would be higher. Assuming particles similar to #1−14, in the terminal velocity regime, are trapped within a cell vesicle with local microviscosity of 140 cP,[35] our magnetic tweezers could move them 10 μm in less than 25 min. In the acceleration regime, the collection time would be less than 3 min. This estimated traveling time is far less than the previously reported value at 8 h,[18] and it shows that real-time manipulation within

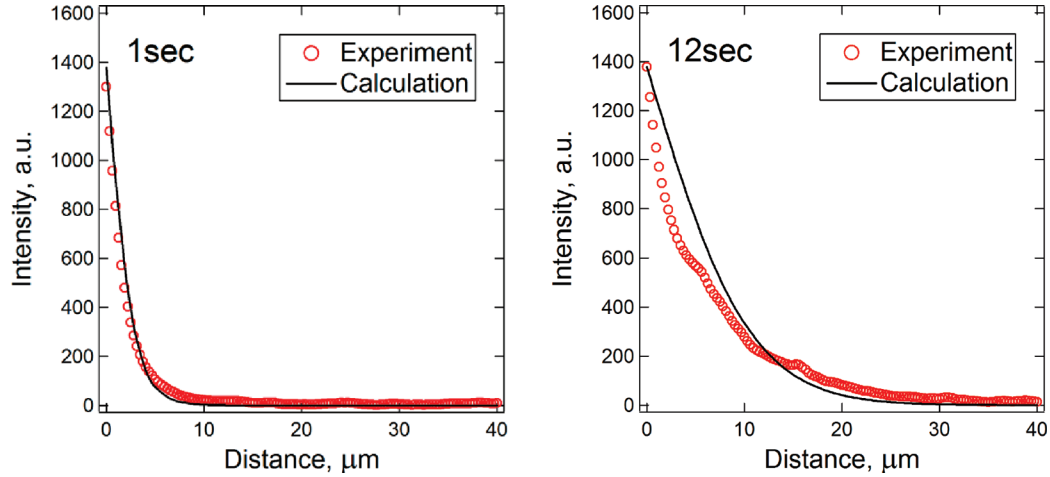

Figure 6. Comparison between the calculated and experimental particle concentration profiles as a function of the distance from the mu metal surface for different times after the solenoid current was turned off. The data are from the images of Figure 5, summed in the vertical direction. The distance plotted here is the distance normal to the surface of the mu metal.

TABLE 1. Overview on the Intracellular Magnetophoretic Response of Different Sizes Particles Subjected to Varying Degree of Magnetic Field Point Source(s)

	diameter of magnetic particles, nm	field gradient, T/m	magnetophoretic force, pN	displacement rate, μm/s
C. Goose and V. Croquette [ref 36]	4500	n.a.	5−20	5
G. H. Basarab, *et al.* [ref 15]	1280	n.a.	500	3
J. S. Kanger, *et al.* [ref 8]	350	8000	5	2.33
this work	38	100−3000	∼0.01	0.05[a]
J. Gao, *et al.* [ref 18]	4	n.a.	n.a.	0.00035

[a]Predicted displacement based on the local microviscosity of 140 cP[35] within the acceleration zone from the magnetic source.

cells is feasible. The ability to distinguish and control magnetic forces as small as 1 fN from viscous and Brownian forces could be an important new tool for detecting binding events and local viscosity variations within cells. Table 1 summarizes our magnetophoresis results and several from the literature. Our combination of larger moment particles than those in Gao's work,[18] plus a large magnetic field gradient, enables us to measure very small forces on single particles by observing their motion in a liquid dispersion. This technique could have useful application in studies of forces within living cells.

EXPERIMENTAL METHODS

An aqueous dispersion of ∼35 nm magnetite particles, coated with a carboxyl group-containing polymer (MW 40 000) was purchased from Ocean Nanotech, Inc. The initial zeta potential, measured with a Malvern Zeta Nanosizer, was −58.4 mV for a Fe concentration of 2.5 mg/mL. Cationic poly(diallyldimethylammonium chloride) (PDDA) with a molecular weight of 100 000−200 000 (20 wt % in water) was purchased from Sigma-Aldrich and used without modification to coat the particles to promote attachment of Au clusters. A 100 μL amount of iron oxide particle solution was added into 10 mL of deionized (DI) water in the presence of 100 μL of PDDA and left to sit overnight until the dispersion was a translucent black suspension. To remove the unadsorbed PDDA, the particles were collected by a permanent magnet, and after decanting, the retantate was redispersed into 10 mL of DI water with intense sonication. Duff's method was employed to make a dispersion of 1.5−3 nm small gold nanoparticles.[25,37] A 100 μL amount of PDDA-coated iron oxide particles was mixed with 6 mL of the Duff's gold dispersion and incubated for 24 h. The particles were then collected by using a permanent magnet and redispersed into 2 mL of DI water with sonication. The particle suspension was further diluted at least 100× for magnetophoresis experiments for optimal dark field illumination. With an estimated ∼20% particle loss at each step of synthesis, the final particle concentration should be ∼0.011 wt %. A low particle concentration is needed for dark field microscopy in order to avoid interference of the plasmonic signals of different particles. The magnetophoresis experiments were conducted with a Zeiss Axiovert 200 inverted microscope with a water immersion objective (Zeiss C-Achromat 20X/1.0 NA) and a Zeiss 1.4 NA universal dark field condenser, oil immersed and in contact with the microscope slide.

Acknowledgment. This material is based on work supported by National Science Foundation grant #CBET 0853963. J.K.L. gratefully acknowledges the financial support from a Dowd-ICES fellowship of Carnegie Mellon University and Fundamental Research Grant Scheme (FRGS/203/PJKIMIA/6071180) from MOHE Malaysia.

Supporting Information Available: Magnetization curve of iron oxide particles, absorbance spectra of iron oxide core, gold-shell nanoparticles, dynamic light scattering measured hydrodynamic diameter distribution of particles at various stages of synthesis, photos of solenoid used and mu metal tip together with its dimensions, a table summarizing magnetophoresis and random walk analysis results, AFM and MFM micrograph of mu metal, and a series of graphs showing the comparison between the calculated and experimental particle concentration profile on the particles released from the mu metal immediately after the solenoid current was turned off. This material is available free of charge *via* the Internet at http://pubs.acs.org.

REFERENCES AND NOTES

1. Grier, D. G. A Revolution in Optical Manipulation. *Nature* **2003**, *424*, 810–816.
2. Prikulis, J.; Svedberg, F.; Kall, M.; Enger, J.; Ramser, K.; Goksor, M.; Hanstorp, D. Optical Spectroscopy of Single Trapped Metal Nanoparticles in Solution. *Nano Lett.* **2004**, *4*, 115–118.
3. Weiss, S. Fluorescence Spectroscopy of Single Biomolecules. *Science* **1999**, *283*, 1676–1683.
4. Chiou, P. Y.; Ohta, A. T.; Wu, M. C. Massively Parallel Manipulation of Single Cell and Microparticles Using Optical Images. *Nature* **2005**, *436*, 370–372.
5. Armani, M. D.; Chaudhary, S. V.; Probst, R.; Shapiro, B. Using Feedback Control of Microflow to Independently Steer Multiple Particles. *J. Microelectromech. Syst.* **2006**, *15*, 945–956.
6. Smith, S. B.; Finzi, L.; Bustamante, C. Direct Mechanical Measurements of the Elasticity of Single DNA Molecules by Using Magnetic Beads. *Science* **1992**, *258*, 1122–1126.
7. Bausch, A. R.; Moller, W.; Sackmann, E. Measurement of Local Viscoelasticity and Forces in Living Cells by Magnetic Tweezers. *Biophys. J.* **1999**, *76*, 573–579.
8. Kanger, J. S.; Subramaniam, V.; Driel, R. Intracellular Manipulation of Chromatin Using Magnetic Nanoparticles. *Chromosome Res.* **2008**, *16*, 511–522.
9. Dobson, J. Remote Control of Cellular Behavior with Magnetic Nanoparticles. *Nat. Nanotech.* **2008**, *3*, 139–143.
10. Ruan, G.; Vieira, G.; Henighan, T.; Chen, A.; Thakur, D.; Sooryakumar, R.; Winter, J. O. Simultaneous Magnetic Manipulation and Fluorescent Tracking of Multiple Individual Hybrid Nanostructures. *Nano Lett.* **2010**, *10*, 2220–2224.
11. Lim, J. K.; Tan, D. X.; Lanni, F.; Tilton, R. D.; Majetich, S. A. Optical Imaging and Magnetophoresis of Nanorods. *J. Magn. Magn. Mater.* **2009**, *321*, 1557–1562.
12. Purcell, E. M. Life at Low Reynolds Number. *Am. J. Phys.* **1977**, *45*, 3–11.
13. Zborowski, M.; Sun, L.; Moore, L. R.; Williams, P. S.; Chalmers, J. J. Continuous Cell Separation Using Novel Magnetic Quadrupole Flow Sorter. *J. Magn. Magn. Mater.* **1999**, *194*, 224–230.
14. Goya, G. F.; Campos, I. M.; Pacheco, R. F.; Saez, B.; Godino, J.; Asin, L.; Lambea, J.; Tabuenca, P.; Mayordomo, J. I.;

Larrad, L.; Ibarra, M. R.; Tres, A. Dendritic Cell Uptake of Iron-Based Magnetic Nanoparticles. *Cell Biol. Int.* **2008**, *32*, 1001–1005.
15. Basarab, G. H.; Karoly, J.; Peter, B.; Ferenc, I. T.; Gabor, F. Magnetic Tweezers for Intracellular Applications. *Rev. Sci. Instrum.* **2003**, *74*, 4158–4163.
16. Anthony, H. B. V.; Bea, E. K.; Roel, D.; Johannes, S. K. Micro Magnetic Tweezers for Nanomanipulation Inside Live Cells. *Biophys. J.* **2005**, *88*, 2137–2144.
17. Lee, C. S.; Lee, H.; Westervelt, R. M. Microelectromagnets for the Control of Magnetic Nanoparticles. *Appl. Phys. Lett.* **2001**, *79*, 3308–3311.
18. Gao, J.; Zhang, W.; Huang, P.; Zhang, B.; Zhang, X.; Xu, B. Intracellular Spatial Control of Fluorescent Magnetic Nanoparticles. *J. Am. Chem. Soc.* **2008**, *130*, 3710–3711.
19. Dunlop, D. J. Magnetite: Behavior near the Single Domain Threshold. *Science* **1972**, *176*, 41–43.
20. Mirowski, E.; Moreland, J.; Zhang, A.; Russek, S. E.; Donahue, M. J. Manipulation and Sorting of Magnetic Particles by a Magnetic Force Microscope on a Microfluidic Magnetic Trap Platform. *Appl. Phys. Lett.* **2005**, *86*, 243901.
21. Pamme, N. Magnetism and Microfluidics. *Lab Chip* **2006**, *6*, 24–38.
22. Yellen, B. B.; Hovorka, O.; Friedman, G. Arranging Matter by Magnetic Nanoparticle Assemblers. *Proc. Natl. Acad. Sci.* **2005**, *102*, 8860–8864.
23. Sahoo, Y.; Goodarzi, A.; Swihart, M. T.; Ohulchanskyy, T. Y.; Kaur, N.; Furlani, E. P.; Prasad, P. N. Aqueous Ferrofluid of Magnetite Nanoparticles: Fluorescence Labeling and Magnetophoretic Control. *J. Phys. Chem. B* **2005**, *109*, 3879–3885.
24. Selvan, S. T.; Patra, P. K.; Ang, C. Y.; Ying, J. Y. Synthesis of Silica-Coated Semiconductor and Magnetic Quantum Dots and Their Use in the Imaging of Live Cells. *Angew. Chem., Int. Ed.* **2007**, *46*, 2248–2452.
25. Lim, J. K.; Eggeman, A.; Lanni, F.; Tilton, R. D.; Majetich, S. A. Synthesis and Single-Particle Optical Detection of Low-Polydispersity Plasmonic-Superparamagnetic Nanoparticles. *Adv. Mater.* **2008**, *20*, 1721–1726.
26. Pallandre, A.; Moussa, A.; Nysten, B.; Jonas, A. M. Nanoconfined Polyelectrolyte Multilayers. *Adv. Mater.* **2006**, *18*, 481–486.
27. Guittoum, A.; Layadi, A.; Bourzami, A.; Tafat, H.; Souami, N.; Boutarfaia, S.; Lacour, D. X-ray Diffraction, Microstructure, Mossbauer and Magnetization Studies of Nanostructured $Fe_{50}Ni_{50}$ Alloy Prepared by Mechanical Alloying. *J. Magn. Magn. Mater.* **2008**, *320*, 1385–1392.
28. Bhusah, B. *Mechanics and Reliability of Flexible Magnetic Media*, 2nd ed.; Springer-Verlag: New York, 2000; pp 52−54.
29. Blumberg, S.; Pennington, M. W.; Meiners, J. C. Do Femtonewton Forces Affect Genetic Function: A Review. *J. Biol. Phys.* **2005**, *32*, 73–95.
30. Yavuz, C. T.; Mayo, J. T.; Yu, W. W.; Prakash, A.; Falkner, J. C.; Yean, S.; Cong, L.; Shipley, H. J.; Kan, A.; Tomson, M.; Natelson, D.; Colvin, V. L. Low Field Magnetic Separation of Monodisperse Fe_3O_4 Nanocrystal. *Science* **2006**, *314*, 964–967.
31. Allwood, D. A.; Xiong, G.; Faulkner, C. C.; Atkinson, D.; Petit, D.; Cowburn, R. P. Magnetic Domain-Wall Logic. *Science* **2005**, *309*, 1688–1692.
32. Vieira, G.; Heninghan, T.; Chen, A.; Hauser, A. J.; Yang, Y.; Chalmers, J. J.; Sooryakumar, R. Magnetic Wire Traps and Programmable Manipulation of Biological Cells. *Phys. Rev. Lett.* **2009**, *103*, 128101.
33. Henighan, T.; Chen, A.; Vieira, G.; Hauser, A. J.; Yang, F. Y.; Chalmers, J. J.; Sooryakumar, R. Manipulation of Magnetically Labeled and Unlabeled Cells with Mobile Magnetic Traps. *Biophys. J.* **2010**, *98*, 412–417.
34. Image processing and analysis in Java http://rsbweb.nih.gov/ij/.
35. Kuimova, M. K.; Botchway, S. W.; Parker, A. W.; Balaz, M.; Collins, H. A.; Anderson, H. L.; Suhling, K.; Ogilby, P. R. Imaging Intracellular Viscosity of a Single Cell during Photoinduced Cell Death. *Nat. Chem.* **2009**, *1*, 69–73.
36. Charlie, G.; Vincent, C. Magnetic Tweezers: Micromanipulation and for Measurement at the Molecular Level. *Biophys. J.* **2002**, *82*, 3314–3329.
37. Duff, D.; Baiker, A. A New Hydrosol of Gold Clusters: 1. Formation and Particle Size Variation. *Langmuir* **1993**, *9*, 2301–2309.